Stanford Exploration Project, Report 80, May 15, 2001, pages 1–143

Transformation of 3-D prestack data by Azimuth Moveout

Biondo Biondi and Nizar Chemingui[1]

ABSTRACT

We introduce a new partial-migration operator, named Azimuth Moveout (AMO), that rotates the azimuth and modifies the offset of 3-D prestack data. AMO can be effectively applied to improve the accuracy and to reduce the computational cost of 3-D prestack imaging. For example, a 3-D prestack dataset can be drastically reduced in size by coherent partial-stacking after AMO. The reduced dataset can be then imaged by prestack depth migration, a process that would have been too expensive to apply to the original dataset. AMO can also be effectively used for regularizing data geometries (e.g. correct for cable feather) and for interpolating unevenly sampled data.

AMO is defined as the cascade of DMO and inverse DMO at different offsets and azimuths. We derive the time-space domain formulation of the AMO operator by first deriving its Fourier domain representation, and then analytically evaluating the stationary-phase approximation. The impulse response of AMO is a surface in the time-midpoint space; the shape of the surface is a skewed saddle, and its spatial extent is determined by the amount of azimuth rotation and offset continuation to be applied to the data. When the azimuth rotation is small ($\leq 20°$), the AMO operator is compact and inexpensive to apply in the time-space domain. We successfully tested AMO by coherently stacking traces with similar offsets and azimuths from a synthetic land survey.

INTRODUCTION

Modern 3-D surveys, both land and marine, have a wide range of offsets and azimuths. Often the offset and azimuth distribution are sub-optimal because acquisition geometry is the result of a compromise between the maximization of data quality and practical and economic constraints. To optimize the imaging of 3-D datasets, it can be useful to modify the effective azimuth and offset distribution of the data during processing, without the need of a detailed a priori assumptions on the underlying velocity function or geology. In this paper we show that this task can be accomplished by applying a partial migration operator that rotates the data azimuth and changes the data absolute offset. Because of its ability to modify the azimuth of the data we have named this operator Azimuth Moveout (AMO).

There are many potential applications for the AMO operator. One of the most promising, and the one that we will illustrate with a synthetic example, is the ability to reduce the amount

[1]**email:** not available

of 3-D prestack data without loss of information by coherently stacking traces that have similar azimuths and offsets. Because the kinematics of 3-D data are dependent on azimuth and offsets, the data needs to be processed with AMO prior to stacking for maximizing coherency among the traces that are averaged. After this data reduction, the application of computationally intensive processes such as 3-D prestack migration becomes more affordable. Another important family of applications is the regularization of data geometries; e.g. the correction for cable feather in marine surveys. After this correction the data can be processed with more efficient algorithms, either because the survey is closer to fulfill 2-D assumptions, or because efficient methods are available for imaging single-azimuth data (Biondi and Palacharla, 1994). Finally, we believe that AMO can be effectively employed for "wave-equation" interpolation of 3-D data (Ronen, 1987) in order to overcome spatial aliasing problems or, more simply, to correct for uneven coverage (Beasley and Klotz, 1992).

The AMO operator can be defined as the cascade of an imaging operator that acts on data with a given offset and azimuth, followed by a forward modeling operator that reconstructs the data at a different offset and azimuth. Any 3-D prestack imaging operator can be used for defining AMO. However, the characteristics of the resulting AMO operator, such as accuracy, cost and degree of required a-priori knowledge of the velocity function, will depend on the choice of the 3-D prestack operator used for its definition. For example, if 3-D prestack depth migration were used to define AMO, the resulting AMO operator would be very accurate. But, on the other hand, it would require a detailed knowledge of the velocity function, and it would be very difficult to derive its analytical representation leading to a potentially expensive implementation. Because of these considerations we have chosen to define AMO from constant-velocity dip moveout (Deregowski and Rocca, 1981; Hale, 1984). We selected DMO for two main reasons. First, DMO is velocity independent, within the well understood limitations of a constant velocity assumption, since it is applied to the data after NMO, which removes the first order effects of velocity variations. Second DMO can be formulated as acting on data with constant offset and azimuth, and thus it naturally lends itself to a straightforward derivation of AMO. Because we derived AMO from DMO, AMO has potentially similar strengths and weaknesses as DMO has. However, we speculate that AMO can be effectively applied when velocity variations are too strong for DMO to successfully continue the data all the way to zero offset. The rationale of this claim, that must be substantiated by further analysis and results, is that the AMO transformation is correct to the first order. Therefore, if AMO is applied when the azimuth rotation and offset continuation are small it should be fairly accurate. However, a generalization of AMO to variable velocity DMO (Perkins and French, 1990; Meinardus and Schleicher, 1993; Hale and Artley, 1993; Popovici, 1994) is likely to be more accurate than the AMO operator presented in this paper.

For some applications, such as the synthesis of 2-D lines from 3-D data, AMO is related to the two-pass 3-D migration proposed by Canning and Gardner (1992), which is based on the successive application of DMO and inverse DMO. However, AMO can be applied to a wider set of problems and datasets because the geometry of the output data is arbitrary. In addition to data regularization, AMO can be applied to data reduction and interpolation. Furthermore, the application of AMO as a single-step procedure can achieve substantial computational savings by exploiting the reduced size of the AMO operator when azimuth rotation and offset

continuation are small.

In the next section we will derive the AMO operator starting from the Fourier domain formulation of DMO (Hale, 1984) and inverse DMO (Ronen, 1987). However, because AMO is intented to be applied to unevenly sampled data a Fourier domain formulation is of little practical interest. Therefore, we derived a time-space formulation of the AMO operator by applying the stationary-phase method to its Fourier expression. The impulse response of the time-space AMO is a skewed saddle surface. The spatial extent of the operator increases with the amount of azimuth rotation and offset continuation that are applied to the data. When the azimuth rotation and offset continuation are small the AMO operator is very compact, and thus is relatively inexpensive to apply as an integral operator.

AZIMUTH MOVEOUT OPERATOR

We define AMO as an operator that transforms 3-D prestack data with a given offset and azimuth to equivalent data with a different offsets and azimuths. Figure **??** shows a graphical representation of this offset transformation; the input data with offset $\mathbf{h}_1 = h_1(\cos\theta_1, \sin\theta_1)$ is transformed into data with offset $\mathbf{h}_2 = h_2(\cos\theta_2, \sin\theta_2)$. AMO is not a single-trace to single-trace transformation, but moves events across midpoints according to their dip. Therefore, AMO is a partial-migration operator, and, since 3-D prestack data is often irregularly sampled, it is most conveniently applied as an integral operator in the time-space domain. For this purpose, in this section we derive a time-space representation of the AMO operator. We first derive the AMO operator starting from the classical definition of DMO in the frequency-wavenumber domain (Hale, 1984) and the definition of its inverse (Ronen, 1987). We then evaluate the stationary-phase approximation of the AMO operator expressed in the frequency-wavenumber domain. The stationary-phase approximation yields a time-space representation of the AMO operator that can be applied as an integral operator. Although, integral AMO can be applied to irregularly sampled data, an accurate implementation of AMO must avoid aliasing of the data and of the operator.

The DMO operator and its inverse, DMO^{-1}, can be defined in the zero-offset frequency ω_0 and midpoint wavenumber $\mathbf{k}$ as

$$DMO = \int dt_1 J_1 e^{-i\omega_o t_1 \sqrt{1+\left(\frac{\mathbf{k}\cdot\mathbf{h}_1}{\omega_o t_1}\right)^2}} \tag{1}$$

$$DMO^{-1} = \int d\omega_o J_2 e^{+i\omega_o t_2 \sqrt{1+\left(\frac{\mathbf{k}\cdot\mathbf{h}_2}{\omega_o t_2}\right)^2}}. \tag{2}$$

The traveltimes t_1 and t_2 are respectively the traveltime of the input data after NMO, and the traveltime of the results before applying inverse NMO. The Jacobians in expressions (1) and (2) can be either the ones proposed in the original Hale's formulation or the improved ones proposed by Zhang (1988). The AMO operator is given by the cascades of DMO and DMO^{-1} and can be written as

$$AMO = \int dt_1 \int d\omega_o J_1 J_2 e^{-i\omega_o\left(t_1\sqrt{1+\left(\frac{\mathbf{k}\cdot\mathbf{h}_1}{\omega_o t_1}\right)^2} - t_2\sqrt{1+\left(\frac{\mathbf{k}\cdot\mathbf{h}_2}{\omega_o t_2}\right)^2}\right)}. \tag{3}$$

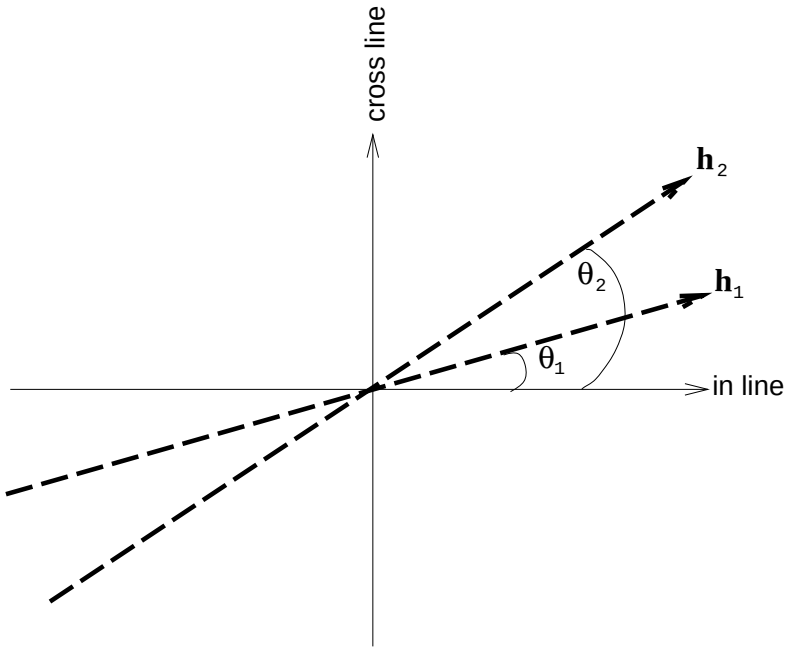

Figure 1: Map view of offset and azimuth of AMO input and output traces. biondo2-sketch [NR]

The derivation of the stationary-phase approximation of the AMO operator is fairly lengthy and complex. We present the outline of this derivation in Appendix A. The equation for the kinematics of the impulse response is,

$$t_2(\mathbf{X},\mathbf{h}_1,\mathbf{h}_2,t_1) = t_1 \frac{h_2}{h_1}\sqrt{\frac{h_1^2\sin^2(\theta_1-\theta_2) - X^2\sin^2(\theta_2-\varphi)}{h_2^2\sin^2(\theta_1-\theta_2) - X^2\sin^2(\theta_1-\varphi)}} \tag{4}$$

while the amplitudes, when Zhang's Jacobian is used, are given by

$$A(\mathbf{X},\mathbf{h}_1,\mathbf{h}_2,t_1) = \frac{\omega_o t_1}{h_1}\frac{\left(1+\frac{X^2\sin^2(\theta_2-\varphi)}{h_1^2\sin^2(\theta_1-\theta_2)}\right)\left(1+\frac{X^2\sin^2(\theta_1-\varphi)}{h_2^2\sin^2(\theta_1-\theta_2)}\right)}{\sqrt{h_2^2\sin^2(\theta_1-\theta_2)-\sin^2(\theta_2-\varphi)}} \tag{5}$$

where $\mathbf{X} = X(\cos\varphi,\sin\varphi)$ is the output location vector in midpoint coordinates. Notice that the zero-offset frequency ω_o enters as multiplicative factor in the expression for AMO amplitudes, but the data is never available as zero-offset data during the AMO process. The effect of this multiplicative factor can be approximated by a time-domain filter applied either to the input or to the output data. For given input half-offset and time ($\mathbf{h}_1$, t_1) and output half-offset ($\mathbf{h}_2$), equations (4) and (5) define a surface in the time-midpoint space. The surface is a skewed saddle; its shape and spatial extent are controlled by the values of the absolute offsets and by the azimuth rotation, i.e.; the differences in azimuths between the input and the output data. Consistent with intuition, the spatial extent of the operator has a maximum for rotation of 90 degrees and vanishes when offsets and azimuth rotation tend to zero. Furthermore, it can be easily verified that $t_2 = t_1$ for the zero-dip components of the data; that is, the kinematics of

zero-dip data after NMO do not depend on azimuth and offset. Figure **??** shows the AMO impulse response for $h_2 = h_1 = 1$ km and azimuth rotation of 30 degrees. The amplitudes of the operator are gray-coded on the surface. The darker the surface, the higher the amplitudes. The rendering of the surface was cutoff for amplitudes lower than 10% of the maximum. Figure **??** shows the AMO impulse response for the same values of the absolute offsets as for Figure **??**, but azimuth rotation of only 10 degrees. As expected, for smaller azimuth rotations the AMO operator becomes much narrower, and the skew of the saddle decreases.

Notice that the expression for the AMO surface is not valid when either h_1 or h_2 are set to zero, or when the azimuth rotation is set to zero. This is not surprising, because in these cases the operator changes from being a surface to be a line. This change in the dimensionality of the operator causes the stationary-phase solution to become singular. However, a different stationary-phase approximation can be derived for these special cases, and the expression of the traveltime curve is then given by the following solutions of a quadric equation

$$t_2(X,h_1,h_2,t_1) = \begin{cases} t_1 \dfrac{\sqrt{2}h_1}{\sqrt{(h_1^2+h_2^2)-X^2+\sqrt{[(h_1-h_2)^2-X^2][(h_1+h_2)^2-X^2]}}} & h_2 \le h_1 \\ t_1 \dfrac{\sqrt{(h_1^2+h_2^2)-X^2+\sqrt{[(h_1-h_2)^2-X^2][(h_1+h_2)^2-X^2]}}}{\sqrt{2}h_2} & h_2 \ge h_1. \end{cases} \tag{6}$$

The width of the operator defined in equation (6) is equal to the difference between the input and output offsets. As expected, the expression reduces to the known expression for integral DMO when the output half-offset h_2 is set to zero and to inverse DMO when input half-offset h_1 is set to zero. Incidentally, equation (6) defines an operator for offset-continuation of 2-D prestack data, and it can have useful applications by its own.

COHERENT PARTIAL STACKING OF A SYNTHETIC 3-D LAND DATASET

AMO can be applied to reduce the data size of a 3-D prestack dataset by coherently stacking traces with similar absolute offsets and azimuths. For example, a land dataset with a wide range of azimuths and offsets can be reduced to a small set of data-cubes with constant offset and azimuth. Then, each of these common-offset cubes can be migrated independently with a 3-D prestack depth migration. The migrated cubes can be stacked together to form the final image, or analyzed to refine the velocity model. To test the application of AMO to this data reduction procedure, we have created a synthetic dataset "recorded" with an idealized land acquisition geometry. The geophones were distributed on a set of parallel lines, and the shots were positioned along lines perpendicular to the geophone lines. The shot and geophone axes were uniformly sampled for achieving equal offset and azimuth distribution for all the midpoints in the central area of the survey. We opted for a regular coverage to analyze the properties of the AMO operator and of our integral implementation in a simple case. But AMO does not require regular geometry; it can actually be used for regularizing data geometries. We modeled the data by a simple Kirchhoff algorithm assuming constant velocity of 2 km/s and a single point diffractor at a depth of 200 meters. The constant velocity assumption was again for the sake of simplicity; tests with a more complex velocity function are required. From this

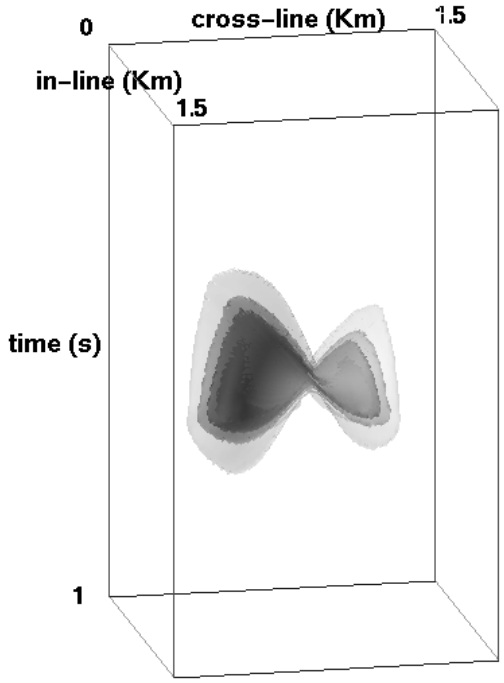

Figure 2: 3-D rendering of AMO impulse response for half-offset equal to 1 Km and azimuth rotation equal to 30°. biondo2-amo-win-30-5 [NR]

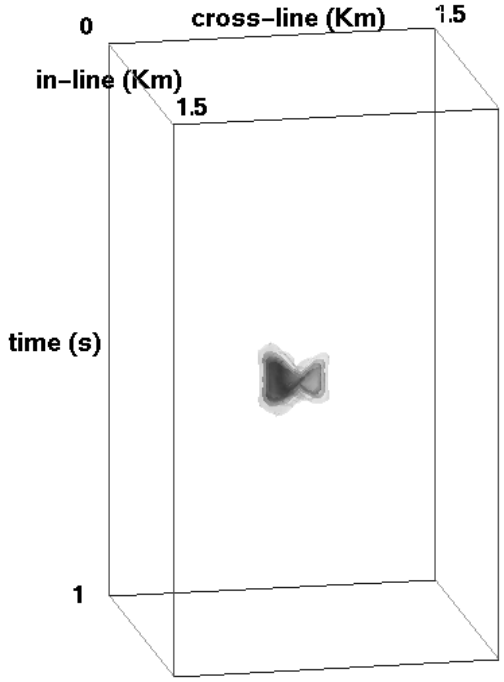

Figure 3: 3-D rendering of AMO impulse response for half-offset equal to 1 Km and azimuth rotation equal to 10°. biondo2-amo-win-10-5 [NR]

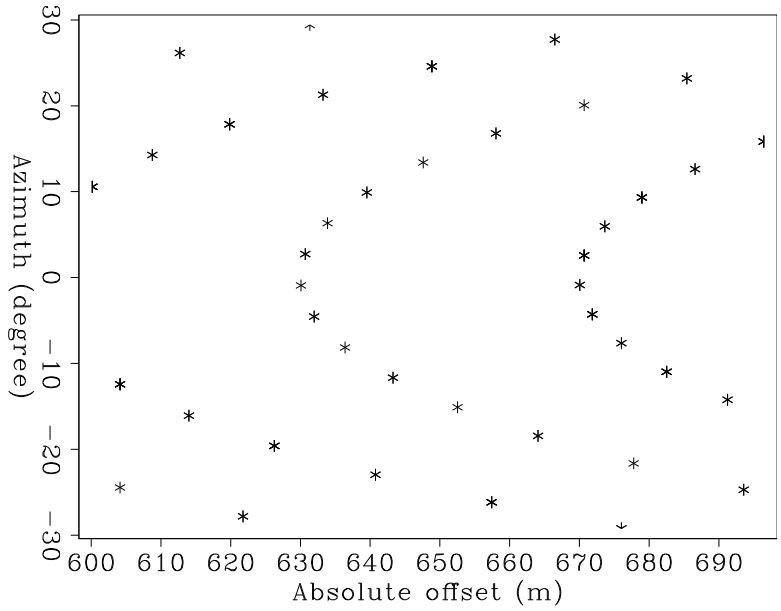

Figure 4: Absolute offsets and azimuths of input-data traces processed by AMO. biondo2-OA [CR]

dataset we synthesized a data cube with one single offset (650 m) and one single azimuth (0°) by applying AMO to all the traces with offset within the (600 m, 700 m) interval and azimuth within the $(-30°, +30°)$ interval. The total number of input traces processed with AMO was about 320,000, and the output cube was made of about 16,000 traces; the reduction factor thus was about 20. Figure **??** shows the absolute offset and azimuth distribution for the input traces that were processed by AMO. Consistently with the theory, AMO was applied after NMO, and inverse NMO was applied after AMO. To check the results of AMO processing we also generated a reference dataset with absolute offset equal to 650 meters and azimuth equal to zero degrees. For comparison, we also computed the result of stacking the same traces after NMO without applying AMO. Figure **??** shows time-slices taken from these three datasets at a constant time of .96 seconds. Between the result of AMO (Figure **??**b) and the reference dataset (Figure **??**a) there are few differences in the frequency content and amplitudes. The AMO results also show artifacts inside the elliptical diffraction curve, but overall, AMO has been successful in reconstructing the prestack data. In contrast, the simple uncoherent stacking process (Figure **??**c) failed to reconstruct the data. The data have lost coherency and, even where the data did stack coherently, the kinematics are wrong. The error in kinematics is larger for the data components dipping along the zero azimuth direction and vanishes along the 90 degree azimuth. The most likely explanation of the artifacts in the AMO results is that our implementation of integral AMO needs a few improvements. Areas that need improvement are the anti-aliasing operator and the transition between the 3-D AMO of equation (4) and the 2-D AMO operator of equation (6).

To gain a better insight into the properties of the AMO operator we show the same three datasets sliced along different directions. Figure **??** shows the vertical slices taken along the in-line direction. The artifacts of the AMO results are clearly visible as well as the inaccuracies

in amplitude along the top of the diffraction curve (Figure **??**b). The kinematics of the result of uncoherent stacking (Figure **??**c) are wrong, except for the zero-dip component of the data. Figure **??** shows the vertical slices taken along the cross-line direction. The kinematics of all three results are similar, though the amplitudes of uncoherent stacking (Figure **??**c) decrease too rapidly with dips. Finally, Figure **??** shows the vertical slices taken along the direction at an angle of 45 degrees with respect to the axis. Uncoherent stacking (Figure **??**c) totally destroyed the data, except for the the zero-dip components.

CONCLUSIONS

The effective offset and azimuth of 3-D prestack data can be modified during the processing flow by applying a partial migration operator (AMO) to the prestack data. We defined the AMO operator in the Fourier domain as the cascade of DMO and inverse DMO. The time-space representation of the AMO operator is then derived by analytically evaluating the stationary-phase approximation of its Fourier representation. The application of AMO in one single step instead of two steps (DMO followed by inverse DMO) leads to substantial computational savings. The AMO operator is compact in space when the azimuth rotation and offset continuation applied to the data are small.

By applying AMO we successfully reduced the data size by a factor of 20 for a synthetic 3-D land survey by performing a coherent partial stack of traces with similar offsets and azimuths. We synthesized a constant offset and azimuth cube from traces with offset varying by up 100 meters and azimuth varying by up 60 degrees.

ACKNOWLEDGMENTS

Discussions with Dave Nichols, David Lumley, and François Audebert have helped to clarify the concept of AMO.

REFERENCES

Beasley, C. J., and Klotz, R., 1992, Equalization of DMO for irregular spatial sampling: 62nd Annual Internat. Mtg., Soc. Expl. Geophys., Expanded Abstracts, 970–973.

Biondi, B., and Palacharla, G., 1994, 3-D prestack migration of common-azimuth data: SEP–**80**, **??**–**??**.

Black, J. L., Schleicher, K., and Zhang, L., 1993, True-amplitude imaging and dip moveout: Geophysics, **58**, no. 1, 47–66.

Bleistein, N., and Handelsman, R. A., 1975, Asymptotic expansions of integrals: Rinehart Winston.

Canning, A. J., and Gardner, G. H. F., 1992, Two pass 3-D prestack depth migration: 63rd Annual Internat. Mtg., Soc. Expl. Geophys., Expanded Abstracts, 892–894.

Deregowski, S. M., and Rocca, F., 1981, Geometrical optics and wave theory of constant offset sections in layered media: Geophys. Prosp., **29**, no. 3, 374–406.

Hale, D., and Artley, C., 1993, Squeezing dip moveout for depth-variable velocity: Geophysics, **58**, no. 2, 257–264.

Hale, D., 1984, Dip-moveout by Fourier transform: Geophysics, **49**, no. 6, 741–757.

Meinardus, H. A., and Schleicher, K. L., 1993, 3-D time-variant dip moveout by the *f–k* method: Geophysics, **58**, no. 7, 1030–1041.

Perkins, W. T., and French, W. S., 1990, 3-D migration to zero offset for a constant velocity gradient: 60th Annual Internat. Mtg., Soc. Expl. Geophys., Expanded Abstracts, 1354–1357.

Popovici, A. M., 1994, Chapter 1: From prestack migration to migration to zero offset: SEP–**80**, 409–424.

Ronen, J., 1987, Wave-equation trace interpolation: Geophysics, **52**, no. 7, 973–984.

Zhang, L., 1988, A new Jacobian for dip moveout: SEP–**59**, 201–208.

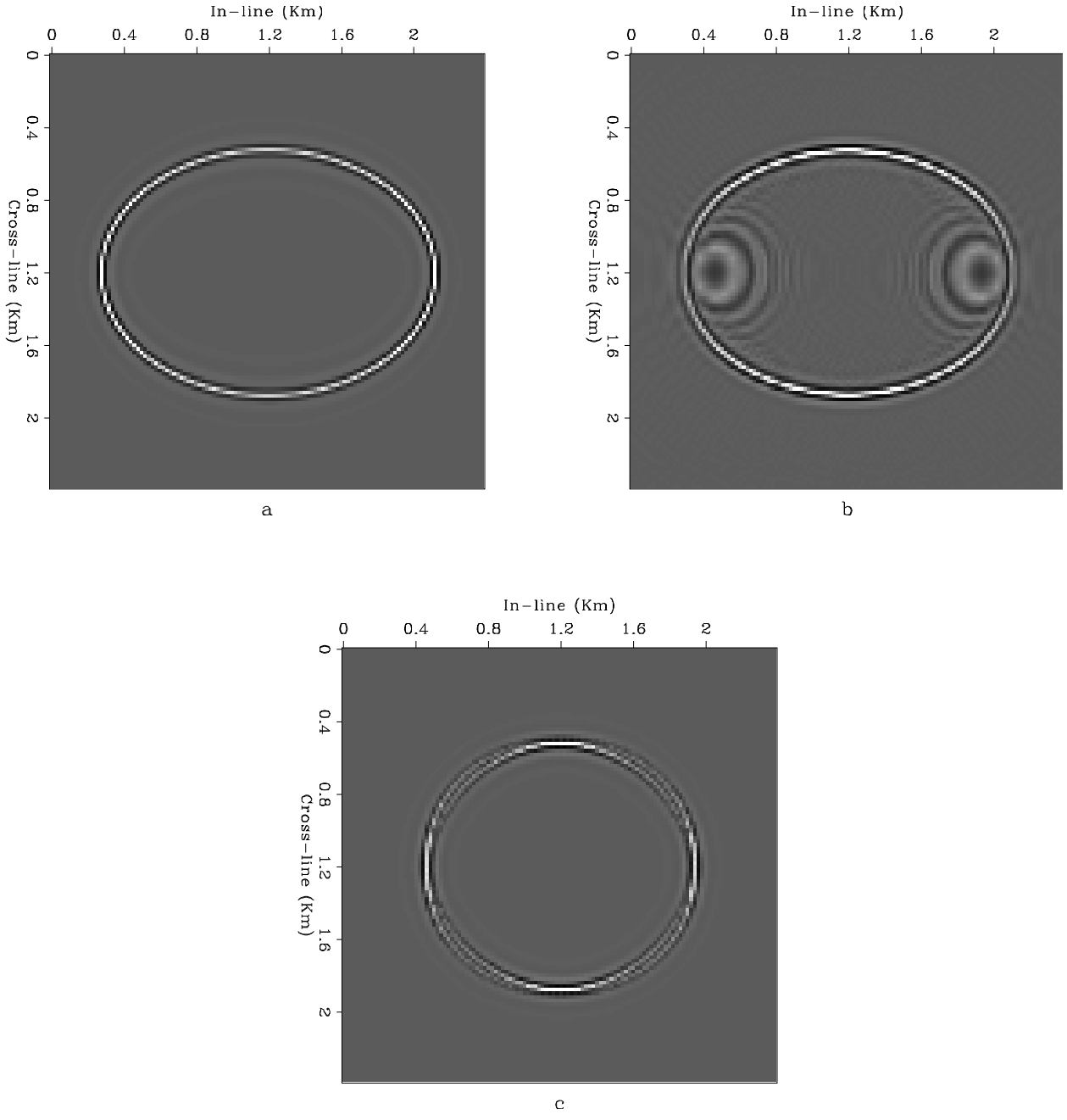

Figure 5: Time-slices taken from: a) the reference dataset, b) the AMO results, and c) the uncoherent stacking results. biondo2-Comp-t [CR]

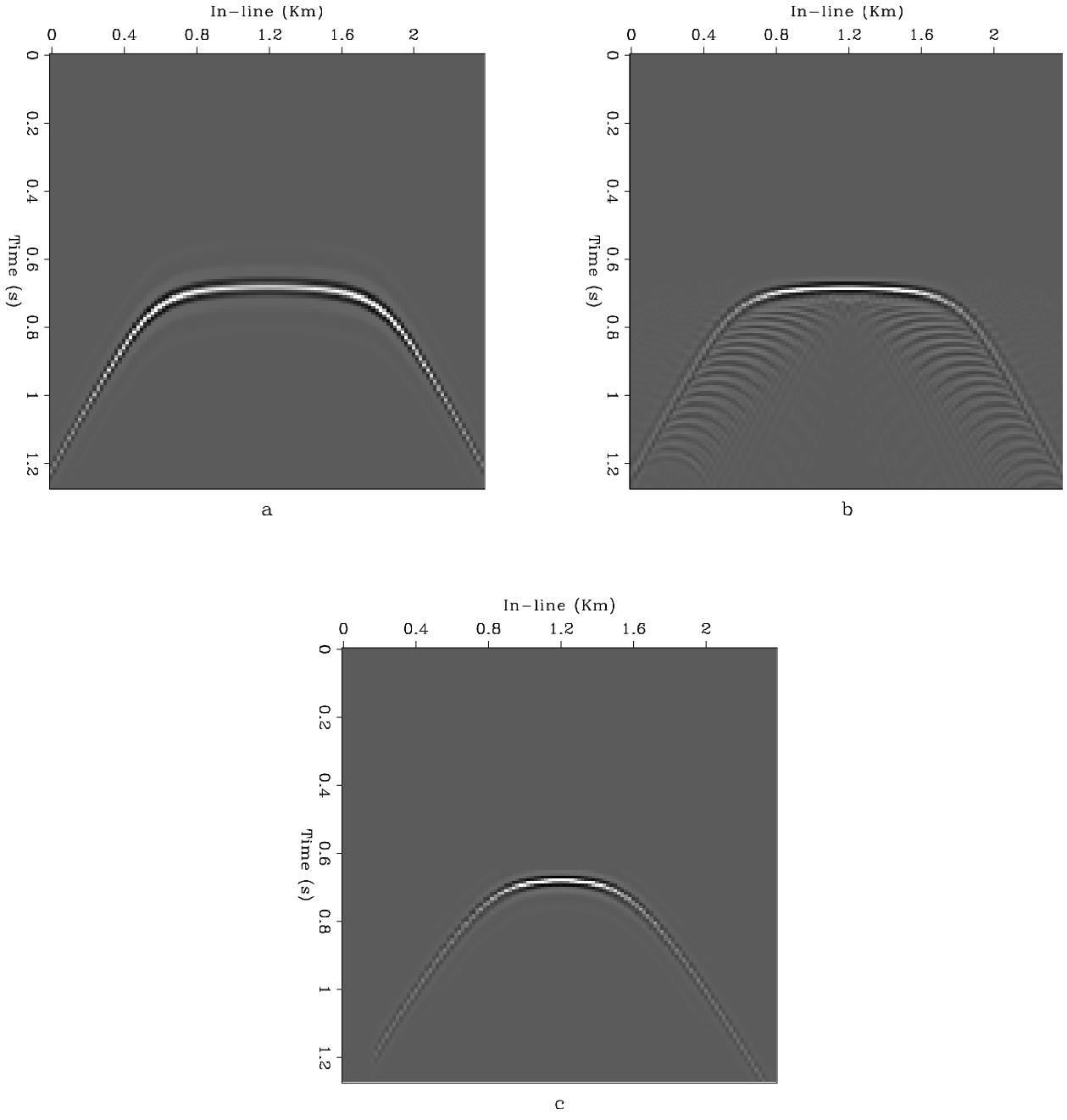

Figure 6: In-line slices taken from: a) the reference dataset, b) the AMO results, and c) the uncoherent stacking results. biondo2-Comp-y [CR]

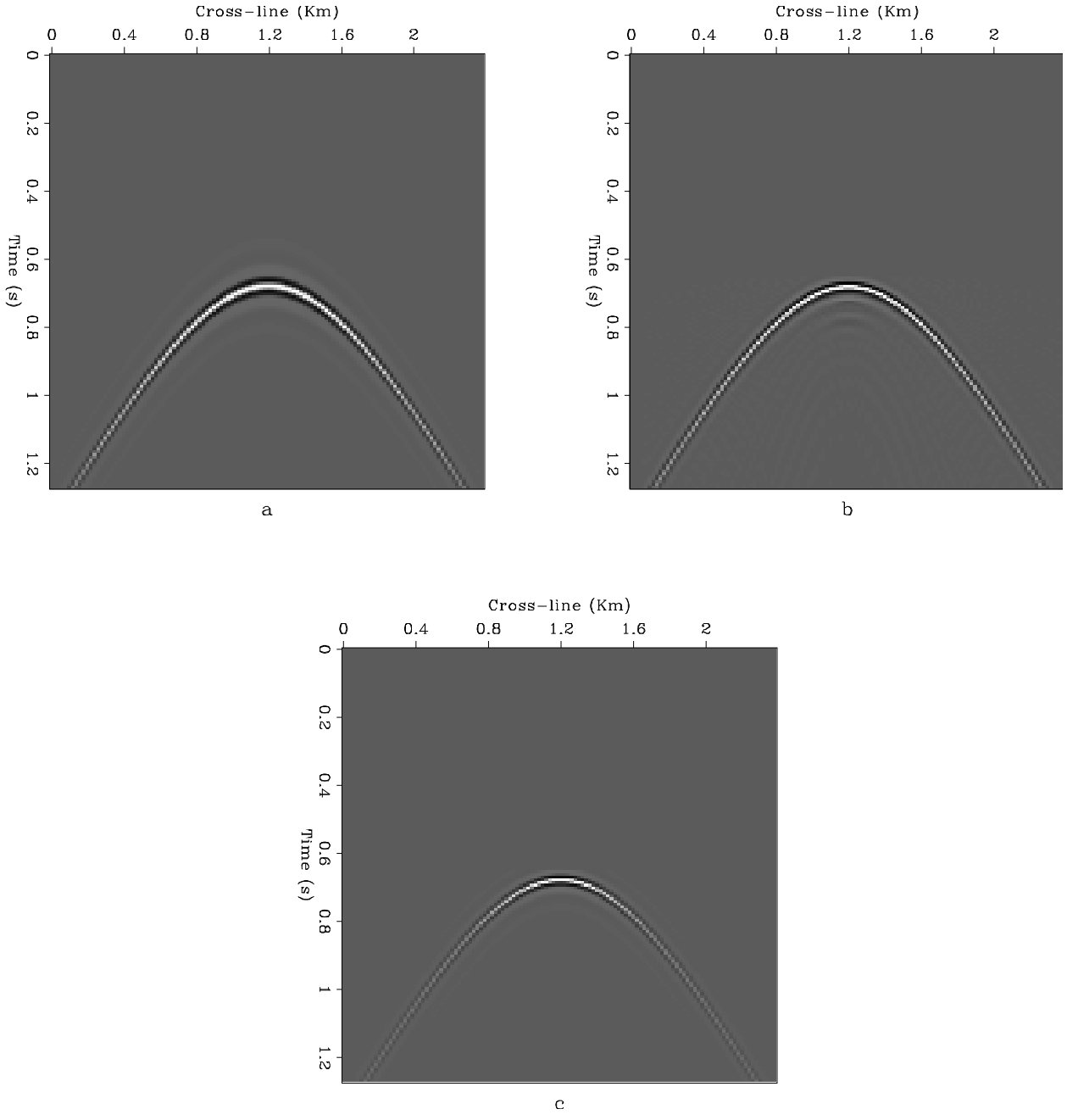

Figure 7: Cross-line slices taken from: a) the reference dataset, b) the AMO results, and c) the uncoherent stacking results. biondo2-Comp-x [CR]

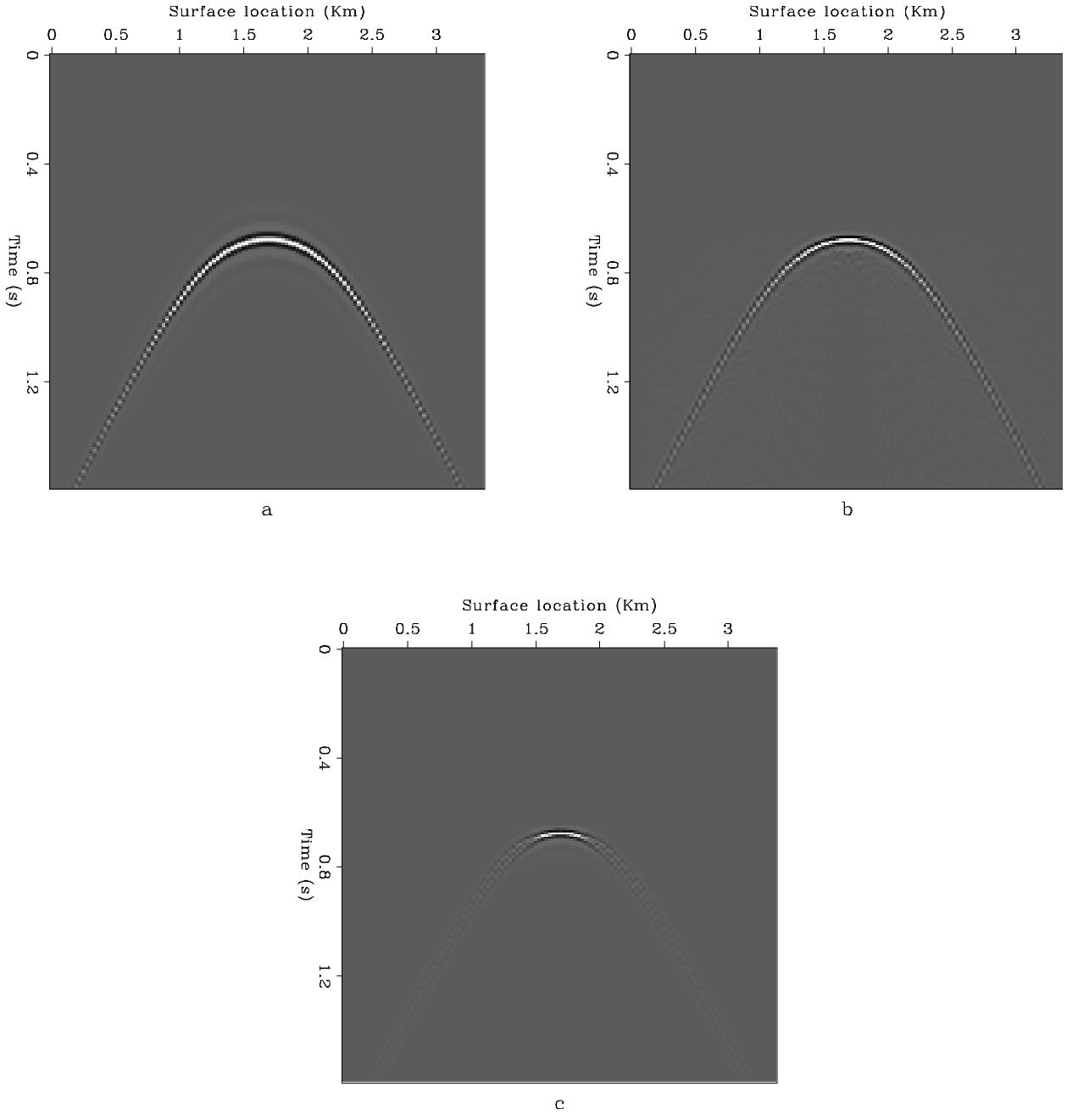

Figure 8: Diagonal slices taken from: a) the reference dataset, b) the AMO results, and c) the uncoherent stacking results. biondo2-Comp-diag [CR]

APPENDIX A

STATIONARY-PHASE EVALUATION OF AMO INTEGRAL

This appendix describes the application of the stationary phase method to approximate the 3-D AMO kernel in the time-space domain. Our derivation has a similar flavor to the stationary-phase approximation of the conventional DMO operator presented in (Black et al., 1993). From equation (3) in the main text, we can write the AMO operator in the time-space domain as

$$AMO = \int\int dk_x dk_y e^{-i(k_x x + k_y y)} \int dt_1 \int d\omega_o J_1 J_2 e^{i\omega_o \left(t_1 \sqrt{1+\left(\frac{\mathbf{K}\cdot\mathbf{h}_1}{\omega_o t_1}\right)^2} - t_2 \sqrt{1+\left(\frac{\mathbf{K}\cdot\mathbf{h}_2}{\omega_o t_2}\right)^2} \right)}, \quad \text{(B-1)}$$

where $\mathbf{X} = x\mathbf{x} + y\mathbf{y} = X(\cos\varphi, \sin\varphi)$ is the output location vector in midpoint coordinates; for sake of notation simplicity we assume that the impulse response is centered at the origin of the midpoint coordinates. We seek to find an approximate solution for the $\mathbf{k}$ integral. We begin by rewriting (B-1) as

$$\begin{aligned} AMO &= \int dt_1 \int d\omega_o \int dk_x dk_y e^{i(\omega_o(t_1\eta_1 - t_2\eta_2) - k_x x - k_y y)} \\ &= \int dt_1 \int d\omega_o \int\int dk_x dk_y e^{i\,\Phi(\omega_o, t, \mathbf{k}, \mathbf{h})}. \end{aligned} \quad \text{(B-2)}$$

The phase of this integral is,

$$\Phi \equiv \omega_o(t_1\eta_1 - t_2\eta_2) - k_x x - k_y y, \quad \text{(B-3)}$$

where,

$$\eta_1 = \sqrt{1+\left(\frac{\mathbf{k}.\mathbf{h}_1}{\omega_o t_1}\right)^2} \qquad \text{and} \qquad \eta_2 = \sqrt{1+\left(\frac{\mathbf{k}.\mathbf{h}_2}{\omega_o t_2}\right)^2}. \quad \text{(B-4)}$$

Next we make the following change of variables and let,

$$\beta_1 = \frac{\mathbf{h}_1.\mathbf{k}}{\omega_o t_1} \qquad \text{and} \qquad \beta_2 = \frac{\mathbf{h}_2.\mathbf{k}}{\omega_o t_2} \quad \text{(B-5)}$$

therefore, η_1 and η_2 become

$$\eta_1 = \sqrt{1+\beta_1^2} \qquad \text{and} \qquad \eta_2 = \sqrt{1+\beta_2^2}. \quad \text{(B-6)}$$

The derivatives of η_1 and η_2 with respect to the wavenumbers k_x and k_y can be written as

$$\begin{aligned} \frac{\partial\eta_1}{\partial k_x} &= \frac{h_{1x}}{w_o t_1}\frac{\beta_1}{\sqrt{1+\beta_1^2}} \qquad \text{and} \qquad \frac{\partial\eta_2}{\partial k_x} = \frac{h_{2x}}{w_o t_1}\frac{\beta_2}{\sqrt{1+\beta_2^2}} \\ \frac{\partial\eta_1}{\partial k_y} &= \frac{h_{1y}}{w_o t_1}\frac{\beta_1}{\sqrt{1+\beta_1^2}} \qquad \text{and} \qquad \frac{\partial\eta_2}{\partial k_y} = \frac{h_{2y}}{w_o t_1}\frac{\beta_2}{\sqrt{1+\beta_2^2}}. \end{aligned} \quad \text{(B-7)}$$

Making one more change of variables, we let

$$\nu_1 = \frac{\beta_1}{\sqrt{1+\beta_1^2}} \qquad \text{and} \qquad \nu_2 = \frac{\beta_2}{\sqrt{1+\beta_2^2}}. \tag{B-8}$$

Setting the derivative of the phase Φ to zero yields the system of equations:

$$\begin{cases} h_{1x}\nu_1 - h_{2x}\nu_2 = x \\ h_{1y}\nu_1 - h_{2y}\nu_2 = y \end{cases} \tag{B-9}$$

which we solve for ν_1 and ν_2 (i.e., η_1 and η_2) at the stationary path $\mathbf{k}_0$. The determinant of the system is given by

$$\Delta = h_{2x}h_{1y} - h_{1x}h_{2y}, \tag{B-10}$$

and the solutions for ν_1 and ν_2 are

$$\nu_{01} = \frac{X\sin(\theta_2-\varphi)}{h_1\sin(\theta_1-\theta_2)}, \tag{B-11}$$

and

$$\nu_{02} = \frac{X\sin(\theta_1-\varphi)}{h_2\sin(\theta_1-\theta_2)}. \tag{B-12}$$

Now we need to evaluate the phase function Φ along the stationary path $\mathbf{k}_0$. By respectively multiplying the equations in (B-9) by k_{0x} and k_{0y} and summing them together we obtain,

$$k_{0x}x + k_{0y}y = \frac{\omega_o t_1 {\beta_{01}}^2}{\sqrt{1+\beta_{01}^2}} - \frac{\omega_o t_2 {\beta_{02}}^2}{\sqrt{1+\beta_{02}^2}}. \tag{B-13}$$

Substituting this relationship into the expression of the phase function [equation (B-3)] we obtain

$$\Phi_0 = \omega_o\left(\frac{t_1}{\sqrt{1+\beta_{01}^2}} - \frac{t_2}{\sqrt{1+\beta_{02}^2}}\right) = \omega_o\left(\frac{t_1}{\eta_{01}} - \frac{t_2}{\eta_{02}}\right). \tag{B-14}$$

The phase function along the stationary path is thus peaked for

$$t_2 = t_1\frac{\eta_{02}}{\eta_{01}} = t_1\frac{\sqrt{1-\nu_{01}^2}}{\sqrt{1-\nu_{02}^2}} \tag{B-15}$$

Substituting equations (B-11) and (B-12) into (B-15) we obtain (4) of the main text;

$$t_2(\mathbf{X},\mathbf{h}_1,\mathbf{h}_2,t_1) = t_1\frac{h_2}{h_1}\sqrt{\frac{h_1^2\sin^2(\theta_1-\theta_2) - X^2\sin^2(\theta_2-\varphi)}{h_2^2\sin^2(\theta_1-\theta_2) - X^2\sin^2(\theta_1-\varphi)}}. \tag{B-16}$$

Next we will derive an expression for the amplitudes of the AMO impulse response. The stationary-phase approximation for the amplitudes of the **k** integral in equation (B-1) is (Bleistein and Handelsman, 1975)

$$A(\mathbf{X},\mathbf{h}_1,\mathbf{h}_2,t_1) \approx \frac{2\pi J_1 J_2}{|det(C)|^{1/2}} e^{i\Phi + sig(C)\frac{\pi}{4}}. \tag{B-17}$$

Therefore we need to evaluate the determinant and the signature of the curvature matrix C, defined as

$$C = \begin{vmatrix} \frac{\partial^2 \Phi}{\partial {k_x}^2} & \frac{\partial^2 \Phi}{\partial k_x \partial k_y} \\ \frac{\partial^2 \Phi}{\partial k_x \partial k_y} & \frac{\partial^2 \Phi}{\partial {k_y}^2} \end{vmatrix}, \tag{B-18}$$

whereas the signature $sig(C)$ is given by the number of positive eigenvalues minus the number of negative eigenvalues. Taking the second order partial derivatives of Φ with respect to k_x and k_y and using the definitions of β_1 and β_2 yields the expressions for $\frac{\partial^2 \Phi}{\partial {k_x}^2}$, $\frac{\partial^2 \Phi}{\partial {k_y}^2}$ and $\frac{\partial^2 \Phi}{\partial k_x \partial k_y}$:

$$\frac{\partial^2 \Phi}{\partial {k_x}^2} = \frac{{h_{1x}}^2}{w_o t_1}(1+\beta_1^2)^{-3/2} - \frac{{h_{2x}}^2}{\omega_o t_2}(1+\beta_2^2)^{-3/2} \tag{B-19}$$

$$\frac{\partial^2 \Phi}{\partial {k_y}^2} = \frac{{h_{1y}}^2}{w_o t_1}(1+\beta_1^2)^{-3/2} - \frac{{h_{2y}}^2}{\omega_o t_2}(1+\beta_2^2)^{-3/2} \tag{B-20}$$

$$\frac{\partial^2 \Phi}{\partial k_x \partial k_y} = \frac{h_{1x} h_{1y}}{w_o t_1}(1+\beta_1^2)^{-3/2} - \frac{h_{2x} h_{2y}}{\omega_o t_2}(1+\beta_2^2)^{-3/2}. \tag{B-21}$$

With a little algebra one may verify that the determinant of the curvature matrix is

$$\begin{aligned} det(C) &= -\frac{(h_{2x}h_{1y} - h_{1x}h_{2y})^2}{\omega_o^2 t_1 t_2}(1+\beta_1^2)^{-3/2}(1+\beta_2^2)^{-3/2} \\ &= -\frac{\Delta^2}{\omega_o^2 t_1 t_2}(1+\beta_1^2)^{-3/2}(1+\beta_2^2)^{-3/2}. \end{aligned} \tag{B-22}$$

We notice that the determinant of C is always negative. Given that the determinant is the product of eigenvalues and C is a two by two matrix, thus C has two eigenvalues which have opposite signs and therefore the signature of C is null.
Using Zhang's (1988) Jacobian, we compute the amplitudes along the surface defined by equation (B-16) that gives the dynamics of the impulse response [equation (5) in the main text];

$$A(\mathbf{X}, \mathbf{h}_1, \mathbf{h}_2, t_1) = \frac{\omega_0 t_1}{h_1} \frac{\left(1 + \frac{X^2 \sin^2(\theta_2 - \varphi)}{h_1^2 \sin^2(\theta_1 - \theta_2)}\right)\left(1 + \frac{X^2 \sin^2(\theta_1 - \varphi)}{h_2^2 \sin^2(\theta_1 - \theta_2)}\right)}{\sqrt{h_2^2 \sin^2(\theta_1 - \theta_2) - \sin^2(\theta_2 - \varphi)}}. \tag{B-23}$$

2-D AMO operator

When the input offset h_1 is parallel to the output offset h_2 the determinant [equation (B-10)] of the system (B-9) is equal to zero. In this case, as we discussed in the main text, the 3-D AMO operator degenerates into a 2-D operator. The fact that the determinant of the system of equations is equal to zero means that the two equations are linearly dependent, and that we are left with only one equation. However, because the operator is two-dimensional, the number of components of the unknown $\mathbf{k}_0$ also goes from two to one. Consequently, another stationary phase approximation to the AMO operator can be found. The new equation is a quartic, and unfortunately, we have not been able to solve this new equation analytically yet. However, we have found the solution for the kinematics of the operator with the help of Mathematica; the resulting expression for the 2-D AMO operator is presented in equation (6) of the main text.